Lasers in Surgery and Medicine 51:390–398 (2019)

The First *In Vivo* Needle-Based Optical Coherence Tomography in Human Prostate: A Safety and Feasibility Study

Abel Swaan, MSc[1,2]* Christophe K. Mannaerts,[1] Berrend G. Muller,[1] Rob AA. van Kollenburg,[1] Marit Lucas,[2] C Dilara Savci-Heijink,[3] Ton G. van Leeuwen,[2] Theo M. de Reijke,[1] and Daniel M. de Bruin[1,2]

[1]*Department of Urology, Amsterdam UMC, University of Amsterdam, Meibergdreef 9, 1105 AZ, Amsterdam, The Netherlands*

[2]*Department of Biomedical Engineering and Physics, Cancer Center Amsterdam, Amsterdam Cardiovascular Sciences, Amsterdam UMC, University of Amsterdam, Meibergdreef 9, 1105 AZ, Amsterdam, The Netherlands*

[3]*Department of Pathology, Amsterdam UMC, University of Amsterdam, Meibergdreef 9, 1105 AZ, Amsterdam, The Netherlands*

Objective: To demonstrate the safety and feasibility of clinical *in vivo* needle-based optical coherence tomography (OCT) imaging of the prostate.

Materials and Methods: Two patients with prostate cancer underwent each two percutaneous *in vivo* needle-based OCT measurements before transperineal template mapping biopsy. The OCT probe was introduced via a needle and positioned under ultrasound guidance. To test the safety, adverse events were recorded during and after the procedure. To test the feasibility, OCT and US images were studied during and after the procedure. Corresponding regions for OCT and biopsy were determined. A uropathologist evaluated and annotated the histopathology. Three experts assessed all the corresponding OCT images. The OCT and biopsy conclusions for the corresponding regions were compared.

Results: No adverse events during and following the, in total four, *in vivo* needle-based OCT measurements were reported. The OCT measurements showed images of prostatic tissue with a penetration depth of ~1.5 mm. The histological-proven tissue types, which were also found in the overlapping OCT images, were benign glands, stroma, glandular atrophy, and adenocarcinoma (Gleason pattern 3).

Conclusions: Clinical *in vivo* needle-based OCT of the prostate is feasible with no adverse events during measurements. OCT images displayed detailed prostatic tissue with a imaging depth up to ~1.5 mm.We could co-register four histological-proven tissue types with OCT images. The feasibility of *in vivo* OCT in the prostate opens the pathway to the next phase of needle-based OCT studies in the prostate. © 2019 The Authors. *Lasers in Surgery and Medicine* Published by Wiley Periodicals, Inc.

Key words: optical coherence tomography (OCT); prostate cancer; diagnosis; Gleason; biopsy

BACKGROUND

Transrectal ultrasound (TRUS)-guided prostate biopsy has been the gold standard in prostate cancer diagnosis for decades. In this procedure, the prostate is sampled with 10–12 biopsies systematically [1]. Ultrasound is used to visualize the prostate during the biopsy procedure, but the ultrasound images cannot accurately visualize prostate cancer (PCa) [2]. Despite the application of systematic multiple core biopsy schemes, clinically significant PCa is often missed or under graded by this method [3]. Also, indolent PCa is frequently diagnosed. Multiparametric magnetic resonance imaging (mpMRI) and targeted biopsy of suspicious "Prostate Imaging Reporting and Data System" (PI-RADS) lesions are, therefore, being used increasingly as studies demonstrate improved detection rates for significant PCa and reduced detection of insignificant cancer [4,5]. The currently used PI-RADS v2 assessment uses a 5-point scale with a score of 1 representing the lowest suspicion and a score of 5 representing the highest suspicion of significant PCa.

As a consequence, mpMRI is currently recommended in men with suspicion of PCa [6–8] . Although mpMRI and mpMRI/TRUS-fusion image targeted biopsy demonstrate good results in experienced hands, a substantial proportion of PI-RADS lesions is false positive, and men with a negative mpMRI cannot be spared systematic biopsy [9]. Definitive diagnosis of PCa is, therefore, still based on the histopathology of prostate biopsy needle cores, often obtained systematically and targeted, instead of imaging only. Biopsies are rated using the Gleason pattern system from 1 to 5; the

Conflict of Interest Disclosures: Dr. Swaan reports grants from NWO-TTW, during the conduct of the study.

*Correspondence to: Abel Swaan, MSc, Amsterdam UMC-AMC, University of Amsterdam, Meibergdreef 9, Rm. L0-112, 1105 AZ Amsterdam, The Netherlands.
E-mail: a.swaan@amc.uva.nl

Accepted 9 April 2019
Published online 14 May 2019 in Wiley Online Library (wileyonlinelibrary.com).
DOI 10.1002/lsm.23093

Gleason score sums the most dominant Gleason pattern with the non-dominant Gleason pattern and biopsies if the malignance has a Gleason score ranging from 6 to 10.

Real-time imaging with information on tissue structure and architecture during prostate biopsy could improve PCa disease characterization and provide a more efficient way of tissue sampling [10]. Optical imaging technologies offer real-time imaging with excellent spatial and temporal resolution and are easily integrated into the operating room. In conjunction with mpMRI/TRUS-fusion targeted biopsy, these real-time technologies in a needle-based form could provide valuable real-time information for tissue characteristics and reduce the currently existing workload of histopathological analysis. Optical coherence tomography (OCT), the light-based equivalent of ultrasound, is capable of visualizing tissue up to ~1.5 mm depth with an axial resolution of 15 μm. Contrast is based on the differences in optical reflectance properties within the tissue. Recent developments have enabled needle integration of OCT that allows for percutaneous access to regions of interest [11]. Recently, an *ex vivo* OCT image atlas has been developed for the prostate based on a near-perfect registration with histology [12]. Based on these results, a protocol has been developed to test needle-based OCT *in vivo* in the prostate [13]. In this study, we demonstrate, for the first time to our knowledge, the safety and feasibility of *in vivo* needle-based OCT imaging of the prostate. The results of four OCT imaging pullbacks in two patients show images with an imaging depth up to ~1.5 mm. Characteristic features, proven by a previous *ex-vivo* study, could be identified in the OCT images. These tissues were afterwards confirmed by the histopathological outcome of the three-dimensional (3D) ultrasound-correlated biopsies. These results are the basis for larger studies in which real-time OCT imaging is performed in a clinical *in vivo* needle-based setting.

METHODS

Study Design

This study is an investigator-initiated, prospective *in vivo* feasibility study, approved by the local institutional review board under registry number: NL57326.018.17. The study is registered on clinicaltrails.gov as Focal Prostate Imaging with CLE and OCT (FPI) (NCT03253458) on August 18, 2017, and the full trial protocol has been previously published [13].

Study Population

Participants were recruited in the Amsterdam UMC, location AMC and were eligible for enrollment if they were planned for a transperineal template mapping biopsy (TTMB) of the prostate. The TTMB was performed in two patients undergoing confirmatory biopsy for focal therapy treatment selection. Both patients gave written informed consent.

Study Procedure

OCT was performed during a template mapping biopsy procedure (Fig. 1) using an Ilumien Optis OCT Intravascular Imaging System combined with a Dragonfly™ OPTIS™ imaging catheter (St. Jude Medical, St. Paul, MN). Two measurement locations per patient were chosen, one aimed at the PCa suspected lesion if visible on mpMRI and one aimed at a lesion-free area. This imaging catheter has a rotating inner part and a 0.9-mm outer diameter, a pullback length of 54 mm, scanning helically at ~90° angle, ~1.5 mm imaging depth, and an axial resolution of 15 μm. The data, which is obtained in 5.4 seconds is real-time visible as 540 cross-sectional images, 1 image per 0.1 mm. The data can be exported as 540 images and as raw OCT data for quantitative analysis.

The Dragonfly probe was interfaced with a trocar needle to enable percutaneous access to the prostate. (Fig. 2) The trocar needle was a 17G co-axial introducer needle that has a length of 16.8 cm (Argon Medical Devices, Athens, TX) and an outer diameter of 1.47 mm.

If available, lesions on mpMRI (Fig. 3a) were used for targeting using cognitive guidance with the real-time ultrasound images. Patients were positioned in the lithotomy position. A clinical ultrasound scanner (VISION Preirus; Hitachi Medical Systems, Tokyo, Japan) with the biplanar probe (EUP-U533; Hitachi Medical Systems) and an endocavity balloon was used for biopsy and OCT guidance. The stepper and grid were placed using a stabilizer mounted on the table. To insert the 0.9-mm OCT probe a 17G trocar needle was used. The tip of the needle was placed at the far end of the measurement trajectory, the inner part of the trocar needle was removed, and the OCT probe was introduced. The outer part of the trocar needle was retracted while the OCT probe stayed at the same position. (Fig. 2b and c) At this point, while the OCT probe was in contact with the surrounding tissue, the pullback imaging procedure was

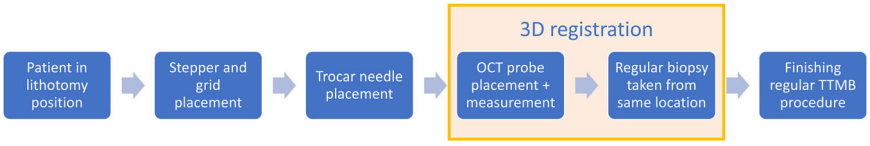

Fig. 1. Flowchart of needle-based OCT measurements during the TTMB procedure. 3D, three dimensional; OCT, optical coherence tomography; TTMB, transperineal template mapping biopsy. [Color figure can be viewed at wileyonlinelibrary.com]

started. (Fig. 2d) Images were exported in a data set of 540 B-scans, one B-scan per 0.1 mm. After the measurement, a standard biopsy was taken from the same location by combining the same grid coordinates and the ultrasound image. The OCT pullback and the biopsy location were both registered by the 3D ultrasound registration software (3DBiopsy, Inc., Aurora, CO) [14]. Hereafter, the regular TTMB procedure was performed, using a 18G biopsy needle with an outer diameter of 1.27 mm.

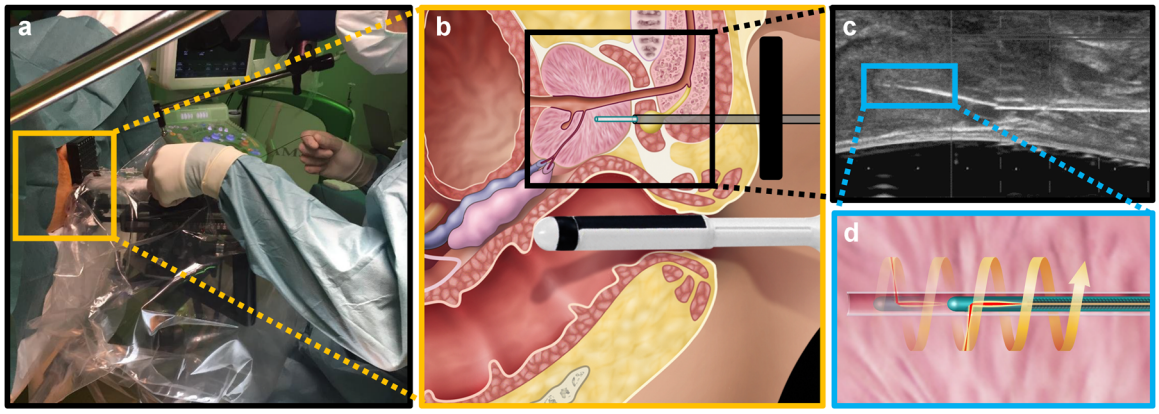

Fig. 2. (a) The OCT measurement with the biplane ultrasound probe and the grid on a stepper. Through the grid, the needle is placed in the prostate, and the OCT probe is slid through the needle. (b) The drawing shows the procedure. (c) The biplane ultrasound probe images the needle and OCT probe. The flexible OCT probe sticking out of the needle is visible. (D) Schematic representation of the OCT measurement. The inner part of the probe rotates and by making a pullback helical measurement of the surrounding prostate tissue can be obtained. OCT, optical coherence tomography. [Color figure can be viewed at wileyonlinelibrary.com]

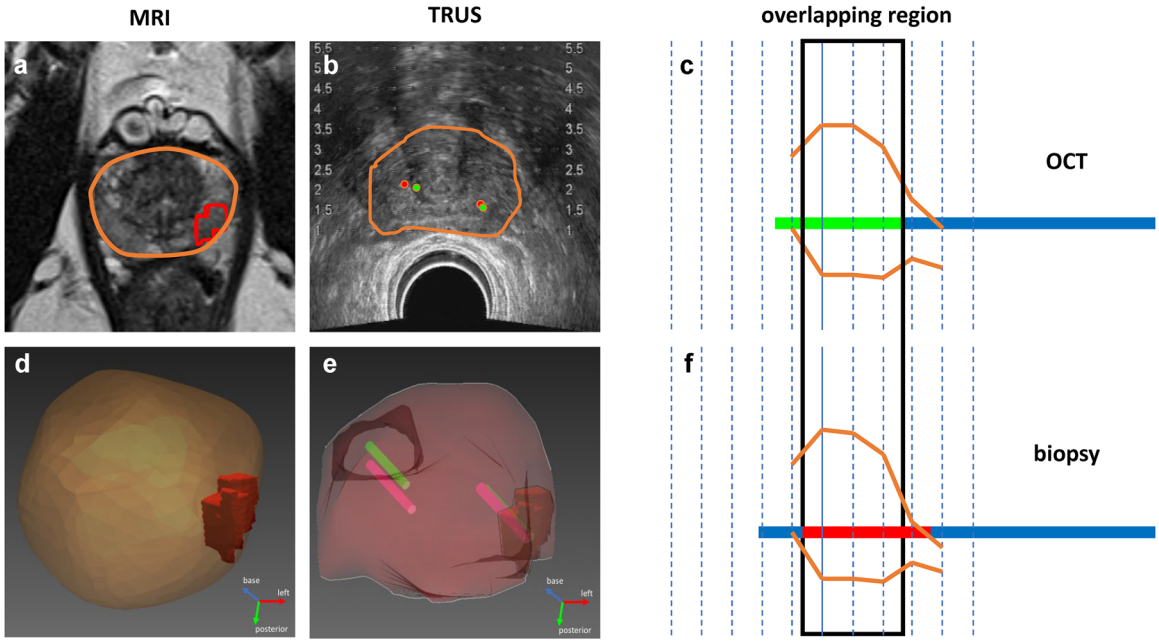

Fig. 3. The prostate in 3D, based on annotations in the transverse mpMRI (a) and TRUS images (b). The transverse T2-weighted mpMRI images were used to annotate the tumor region (red), which resulted in a 3D volume (red) in the 3D prostate image (d). The transverse (b) and longitudinal (c and f) TRUS images were used to annotate the prostate (boundary depicted by the orange line) and to register the OCT measurement (c) and biopsy locations (f). The mpMRI-based 3D tumor volume is overlaid on the 3D TRUS image (e, red volume) combined with the 3D registration of the OCT (green) and biopsy locations (pink). The overlapping region depicted in (c) and (f) is used for the co-registration of the OCT images with the biopsy. 3D, three dimensional; mpMRI, multiparametric magnetic resonance imaging; OCT, optical coherence tomography; TRUS, transrectal ultrasound. [Color figure can be viewed at wileyonlinelibrary.com]

Safety and Feasibility

Safety was tested by observing the patients on adverse events during the procedure and on immediate follow-up. Feasibility was described by scoring OCT device malfunction, procedural failures, and OCT data quality.

Histological Evaluation

Histological evaluation was performed and reported by a uropathologist (CS-H) using digitally scanned images of the pathology slides. After regular diagnosis during clinical routine, the uropathologist annotated regions containing different tissue types on the high-resolution scans of the histology slides, which corresponded with the OCT pullbacks, using an in-house build annotation software. The nine different tissue types (cystic glandular atrophy, regular glandular atrophy, benign glands, fat-tissue, adenocarcinoma [Gleason pattern 3/4/5], fibromuscular stroma, and inflammation) were annotated if present.

Matching and Comparing OCT With Histology

The biopsy needle and the OCT probe (Fig. 2c), which were clearly visible on the ultrasound during the procedure, were manually registered with the 3Dbiopsy software (Fig. 3b). Both, the biopsy and the OCT, were taken from the same location. Within the resulting overlapping region (Fig. 3c and f), the pathological findings were compared with the co-localized OCT images. All OCT images were categorized by three trained experts (BM, RvK, and AS) in one of the following tissue types: cystic atrophy, regular atrophy, benign glands, fat, Gleason pattern 3, 4, or 5, stroma, and inflammation. The OCT images with unrecognizable or multiple tissue types were discarded. After the individual categorization, a consensus was reached. If no consensus was reached, the OCT data was excluded from further analysis.

Comparing *In Vivo* OCT With Atlas

Typical *in vivo* OCT examples, resulting from the histology matched OCT images, were compared with the previously published *ex vivo* atlas images of Muller et al.[12] *In vivo* OCT features of the different tissue types were described and compared with the *ex vivo* OCT features.

RESULTS

Patient Characteristics

From May to June 2018, two patients were recruited for the study and underwent OCT imaging during TTMB. Both patients had biopsy-proven PCa diagnosed elsewhere and were referred to our center for confirmatory biopsy to determine the treatment eligibility for focal therapy (irreversible electroporation) of the prostate.

The first patient had a mpMRI of the prostate that demonstrated a PI-RADS four lesion of 13 mm in length in the dorsolateral side of the peripheral zone in the left apex with no signs of capsular invasion or seminal vesicle invasion (Fig. 3). The previous biopsy showed a PCa Gleason $3 + 4 = 7$ in 1 out of 8 biopsies. In the second patient, the mpMRI of the prostate was scored as PI-RADS 2, and no tumor focus was recognizable. However, motion artifacts and blood residue could have diminished the reading. The previous biopsy showed a PCa Gleason $3 + 4 = 7$ in 1 out of 11 biopsies.

Safety and Feasibility

Two locations in the prostate were measured by OCT. To be certain, a second measurement at both locations was performed without repositioning the probe.

No adverse events were reported during and following the procedure. Introducing one OCT needle in our current research setting took about 3 minutes, including cognitive fusion of the MRI with the United States. While each OCT measurement only took 5.4 seconds, the overall extra time for OCT procedure time was 17 minutes for patient 1 and 16 minutes for patient 2.

No device malfunctions were reported while acquiring OCT measurements. The OCT measurements were evaluated for significant artifacts during the procedure. No procedural failures were reported during the procedure. All acquired data sets were visualized during the procedure and contained high-quality data over the full pullback. Subsequent off-line evaluation of the measurements showed some minor artifacts in the flushing canal around the inner part of the probe.

Histological Evaluation

Patient 1. Based on the prostate volume of 34 mL, on ultrasound, a 20-core TTMB was performed. Two out of the 20 biopsy cores were positive for adenocarcinoma. One core contained a Gleason score $3 + 4 = 7$ adenocarcinoma of the prostate (the transition zone posterior of left apex), while the other core contained a Gleason score $3 + 3 = 6$ adenocarcinoma of the prostate (the dorsolateral peripheral zone of the left apex). In both biopsy cores, tumor percentage was approximated as occupying more than 50% of the biopsy volume.

Patient 2. Based on the prostate volume of 61 mL, based on ultrasound, a 30-core transperineal template mapping biopsy was performed. One out of the 30 biopsy cores was tumor positive. This core of the dorsolateral peripheral zone of the left apex contained a Gleason score $3 + 4 = 7$ adenocarcinoma of the prostate with a tumor core infiltration of more than 50% of the biopsy volume.

Matching and Comparing OCT With Histology

After an individual evaluation of the four OCT measurements by the OCT experts, based on their *ex vivo* OCT knowledge, seven different tissue types were found: benign glands, cystic atrophy, regular atrophy, Gleason 3, Gleason 4, stroma, and inflammation. These seven tissue types were also identified in the histopathology slides. However, after identification of the overlapping region between OCT measurements and histopathology slides, only parts of the OCT data sets could be used: 58% for OCT 1, 76% for OCT 2, 87% for OCT 3, and 35% for OCT

4. As a result, Gleason 4 was identified by OCT outside the overlapping region. Furthermore, inflammation and cystic atrophy could not be matched between the OCT measurements and the histopathology findings of the corresponding overlapping region (Table 1). Thus, only four tissue types were present in OCT images and corresponding histopathology slides of these regions: regular atrophy, benign glands, Gleason 3, and stroma; vice versa, cystic atrophy, regular atrophy, and inflammation were identified in the OCT measurements of the overlapping region but not in the corresponding histopathology slices. Please note that perfect matches were not to be expected: OCT images containing multiple tissue types were omitted in the analysis and histopathology slices only represent a small part of the biopsy. As an example, in Figure 4c and d two cross-sectional OCT images are displayed from the overlapping region in Figure 4b. In Figure 4c, the imaging depth is measured. Tissue structures are visible at 10 to 2 o'clock within the line-dot circle, which is drawn at 1.5 mm in depth.

Comparing *In Vivo* OCT With Previously Published Atlas Data

Features of the four different tissue types, which were identified on OCT and matched with histology, were compared with the images from the *ex vivo* study [12]. The *ex vivo* and *in vivo* images are combined in Figure 5, demonstrating the similarities and differences in the characteristic features (Table 2). OCT images containing multiple tissue types were omitted.

DISCUSSION

In this study, we demonstrated that *in vivo* OCT imaging of the prostate is feasible. The OCT measurements, which extended the procedural time by approximately 15 minutes, did not cause any technical issues and adverse events during and following the intervention, which indicates that the procedure seems safe as well.

After analyzing the images in the study, we observed distinguishable features up to a maximum depth of ~1.5 mm. Still, some small artifacts were observed inside the flushing channel of the OCT probe, which most probably can be attributed to blood or air bubbles caused by the moving needle and OCT probe during positioning. We expect that additional flushing will reduce the artifacts. Bleeding outside the probe was not observed in the OCT images, probably because tissue is merely pushed aside, and no tissue is removed from the prostate at the time of measurement. The difference between taking tissue by a regular biopsy versus going in and out while pushing tissue aside with an OCT probe can have a different effect on the bleeding in the prostate, which should be investigated in future studies. The long measurement trajectory of the OCT probe (54 mm) and ~1.5 mm penetration depth result in a significant advantage over regular biopsies; the maximum volume of visualized tissue with one OCT measurement is 600 mm^3. This volume is ~14 times larger than the potential volume of the biopsy with a 1-mm diameter over the same length. The following calculations were used to measure the OCT and biopsy volumes, taking into account the volume of the OCT probe: volume $OCT = (\pi \cdot 1.952 - \pi \cdot 0.452) \cdot \text{length} = \sim 11.30\ mm^2 \cdot \text{length}$, volume $\text{biopsy} = \pi \cdot 0.52 \cdot \text{length} = \sim 0.79\ mm^2 \cdot \text{length}$. An additional advantage is that the long OCT pullback can visualize the peripheral and anterior zone within one measurement.

In vivo OCT images will always be more difficult to correlate with histology than studies with *ex vivo* OCT images [12,15,16]. Not all the OCT images could be correlated one-to-one to histology, which can be attributed to the discrepancies in volume between the OCT and biopsy, the unknown orientation of the biopsy, and the co-localization mismatches. The histology from OCT pullback # 1 contained five different tissue types, of which benign glands and Gleason 3 pattern adenocarcinoma were independently identified in both OCT and histology. Regular atrophy, Gleason pattern 4 adenocarcinoma, and stroma were probably not found because of exclusion of B-scans containing multiple tissue types and similarities between Gleason 3 and 4 patterns on OCT. OCT pullback #2 was found to be matched with three

TABLE 1. Correspondence between the histopathological and OCT findings in the overlapping regions

Pt	Tumor volume % of prostate cancer in the biopsy based on histology	OCT	Benign glands (OCT/ biopsy)	Cystic atrophy (OCT/ biopsy)	Regular atrophy (OCT/ biopsy)	Gleason pattern 3 (OCT/ biopsy)	Gleason pattern 4 (OCT/ biopsy)	Stroma (OCT/ biopsy)	Inflammation (OCT/biopsy)
1	50%	1	Yes/Yes	Yes/No	No/Yes	Yes/Yes	No/Yes	Yes/Yes	Yes/No
	0%/No PCa	2	Yes/Yes	No/Yes	Yes/Yes	No/No	No/No	Yes/Yes	No/Yes
2	50%	3	Yes/Yes	No/No	Yes/No	Yes/Yes	No/Yes	No/Yes	No/No
	0%/No PCa	4	Yes/Yes	No/No	No/Yes	No/No	No/No	Yes/Yes	No/No

OCT, optical coherence tomography; PCa, prostate cancer.
"No PCa" indicates that no prostate cancer was found in the histologic biopsy specimen. Please note that OCT images containing multiple tissue types were omitted. Yes/Yes indicates that the tissue was present in the OCT data and in the biopsy data. Yes/No indicates that the tissue was present in the OCT data but not in the biopsy data. No/Yes indicates that the tissue was not present in the OCT data but was present in the biopsy data. No/No indicates that the tissue was neither present in the OCT data nor in the biopsy data.

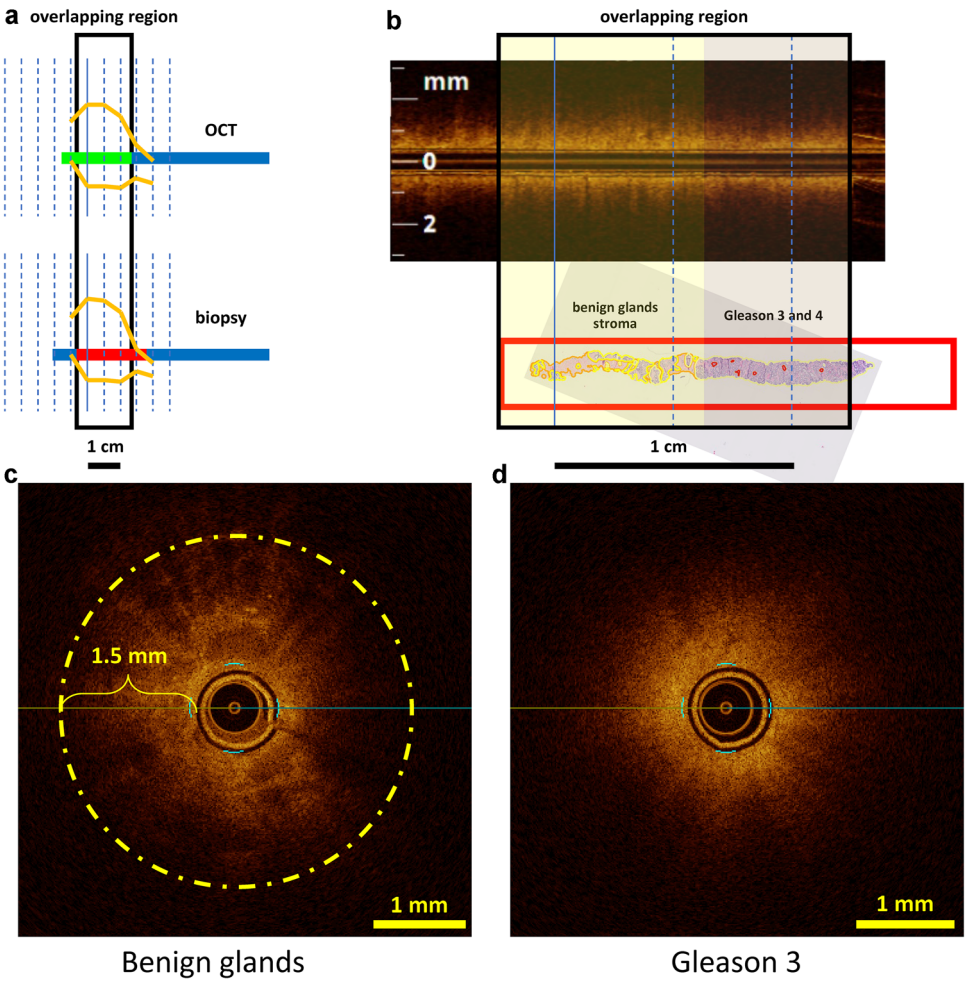

Fig. 4. The overlapping region of the corresponding regions. Left (a) the OCT measurement and biopsy position based on the longitudinal ultrasound image of the prostate (orange), captured with the 3Dbiopsy software. Based on this measurement the overlapping region of the OCT measurement and biopsy can be defined. On the right (b), the overlapping region of the OCT measurement and the biopsy are placed next to each other. The biopsy needle length is 20 mm, the biopsy itself is, in this example, 15 mm. The location of the biopsy should be somewhere inside the red box. The findings of the pathologist were, in this case, benign glands and stroma on the left and Gleason 3 + 4 on the right. Corresponding OCT B-scan of benign glands (c) and Gleason 3 (d), evaluated by the trained OCT reviewers, are displayed below. Please note that structures in image C are still visible at a depth of 1.5 mm (line-dot circle) from the probe. However, this imaging depth is dependent on the tissue scattering properties. OCT, optical coherence tomography. [Color figure can be viewed at wileyonlinelibrary.com]

tissue types with the corresponding biopsy. Cystic atrophy and inflammation were identified in the biopsy, not in the OCT. In the histology corresponding to OCT pullback #3, benign glands, regular atrophy, and Gleason 3 and 4 patterns were diagnosed. However, on OCT pullback #3 we did not recognize the small islands of Gleason 4 pattern (red spots in Fig. 4). The visual difference between Gleason 3 and 4 is small, which makes it difficult to differentiate these tissues on OCT [12]. By comparing OCT pullback #4 with the corresponding histology slide, we were able to identify the benign glands and stroma but could not determine the regular atrophy.

Mismatches are probably due to the heterogeneity of the prostatic tissue. Sometimes multiple tissue types were recognized on one B-scan, which were subsequently excluded for correlation. Also, the OCT images were rated by three reviewers who all had an *ex vivo* prostatic OCT images training set.

The lack of perfusion can change the tissue characteristics, which is also suggested by Dangle et al.[15] in the postprostatectomy *ex vivo* study to spot positive margins. This variation of tissue characteristics impedes the identification of *in vivo* tissue characteristics, which were identified and learned using *ex vivo* images. To rate *in vivo* OCT images, a training set of *ex vivo*

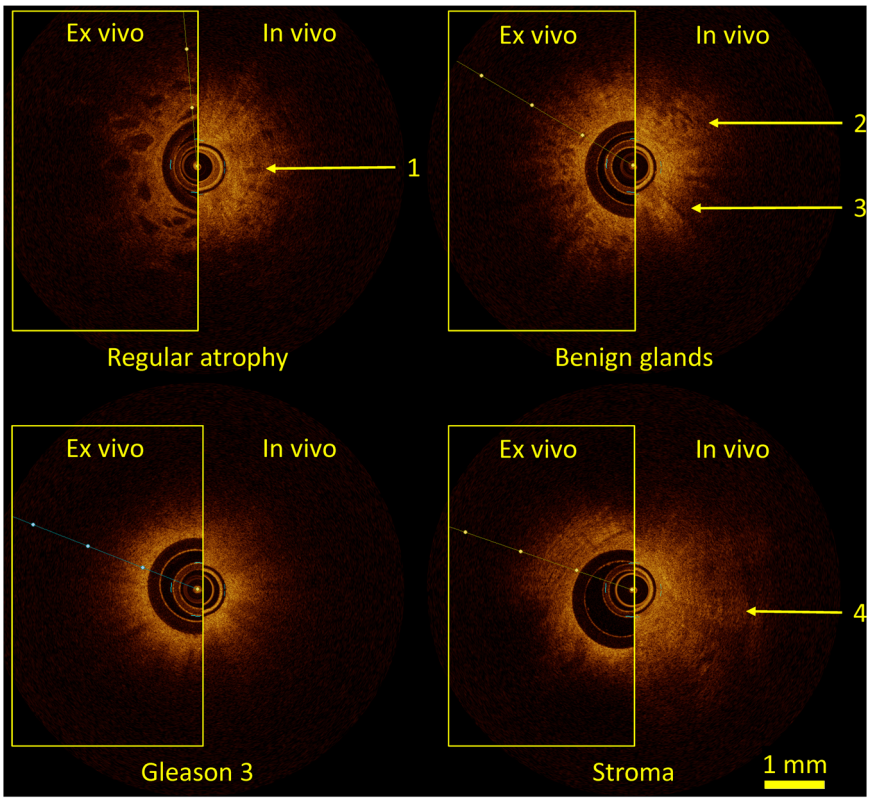

Fig. 5. *In vivo* and *ex vivo* atlas OCT atlas of typical examples of the different tissues, *ex vivo* images are in the yellow boxes. The *in vivo* OCT images visible in this atlas are located in overlapping regions Figure 4 of one of the four OCT pullbacks. The arrows with the number identify the features given in Table 2. Please note that because of the measurement setup, the *ex vivo* images have an extra tube around the probe, which resulted in an extended distance between the center of the probe and the tissue. OCT, optical coherence tomography. [Color figure can be viewed at wileyonlinelibrary.com]

OCT images is not ideal. Also, we do not know the learning curve of classifying *in vivo* OCT images. These learning curves have to be determined in a similar setup as was done for classifying the PCa on mpMRI [17,18].

A large inter-observer variance exists for the classification of prostatic tissue. Consequently, OCT images can be mismatched. In our study, the histological evaluation and delineation were performed by one experienced uropathologist only. Future studies should include more pathologists

TABLE 2. Description of *ex vivo* and *in vivo* features found in the different tissue types

Tissue type	Visual OCT features *ex vivo*[12]	Visual OCT features *in vivo*
Regular atrophy	Smaller (0.1–0.3 mm), dark, more grouped cavities compared to cystic atrophy	Smaller ~0.1 mm, *less scattering*, grouped cavities (1). Light penetrates to medium range in the tissue.
Benign glands	Smaller, mostly grouped cavities (≤0.1 mm), cavities could be dark or opaque	Irregular scattering tissue with small dark (no scattering) round cavities (2) with a few spiked shadows (3)
Gleason 3	Homogeneous tissue structures. High signal surrounding the probe and low signal in depth represented a low signal penetration (<1 mm), probably due to a high cell density	Similar to *ex vivo*: Homogeneous tissue structures. High signal surrounding the probe and low signal in depth represented a low signal penetration (<1 mm)
Stroma	Homogeneous tissue with an increased signal depth (≥1 mm). Unique: parallel ellipsoidal-shaped lines (4) on both sides of the probe	Similar to *ex vivo*, *deeper light penetration*. The unique parallel ellipsoidal-shaped lines (4) are visible, yet less visible compared with *ex vivo*

OCT, optical coherence tomography.
Second column is modified from Muller et al. [12] The numbers identify with the arrows in Figure 5 at different visual OCT features.

with a final consensus in the diagnosis and delineation to reduce the disparity within the histological tissue [19].

Previously, utilization of non-needle-based *ex vivo* OCT of prostatic biopsies has been described in several studies. Jain et al.[20] reported four different tissue types in an *ex vivo* rodent prostate using full field OCT (ffOCT). Although two reported tissue types showed similar features as in our results, it's difficult to visually compare the images due the differences in acquisition methods. Beuvon et al.[21] in a pilot study and Lopater et al.[22] in a more extended study reported on a ffOCT visualization of human prostate biopsy specimens, which was correlated to histology. For the latter study, a promising average accuracy for cancer detection of high Gleason score (>3 + 3) of 72% was reported. Nonetheless both studies only describe the detection of cancer versus healthy tissue and do not describe OCT-specific features for tissue classification. Previously published results on prostate OCT imaging by Dangle et al.[15] showed the visualization of surgical margins in 100 prostatectomy specimens compared with histopathology. The probe-based time domain OCT system was primarily developed for the detection of bladder cancer. In this study, it was demonstrated that the negatives predictive value of OCT for the detection of surgical margins was 96%, showing the potential of *in vivo* OCT for the detection of cancer.

Comparing *In Vivo* OCT With Previously Published Atlas

The *in vivo* images contain comparable features as the *ex vivo* OCT images from the previous study.[12] Differences of *in vivo* and *ex vivo* images were found in the regular atrophy where the lumens appeared to be smaller. Benign glands showed its characteristic cavities with a few thin shadows. The differentiation between regular atrophy and benign glands seemed to be more challenging in *in vivo* tissue than in *ex vivo* tissue. Probably, compared with the *ex vivo* obtained OCT images, during the *in vivo* measurements, the perfusion of the prostate and the induced pressure result in smaller cavities in regular atrophy.

Different from our previous *ex-vivo* studies,[12,23,24] the light seems to penetrate deeper *in vivo* for stroma compared with the Gleason patterns. This difference in penetration depth should be exploited in future studies by determining the optical attenuation coefficient.[12,23,24]

The possibility of collecting good quality images of the prostate with needle-based OCT measurements is now the first successful step towards a larger cohort study that aims to correlate OCT with histology to set up *in vivo* discriminative parameters.[13] By using two highly selected patients with PCa prior to this proposed correlation study, we follow the IDEAL recommendations [25]. Distinguishing some tissue types with OCT is possible. If needle-based OCT can differentiate tumor tissue from the other prostate tissues, it would have an impact on PCa diagnosis in the clinic. First, the large "sampling" volume of the OCT scan needs fewer punctures than using the traditional biopsy. Second, the diagnosis can be given real-time, that is, the urologist or uropathologist can see the OCT images while the probe is still in the patient. This real-time diagnosis could enable the same-day minimal invasive treatment and might reduce the patient's burden.

The layers of the OCT images can also be analyzed by deep learning algorithms, as is performed in the retina by De Fauw et al.[26] Besides layers analysis, quantitative analysis in combination with deep learning algorithms could speed up and enhance the accuracy of tissue classification. The volume of the diagnostic images is increasing rapidly. With these instant, accurate results, we might be able to deliver immediate treatment of the suspected lesions, for example, by laser therapy through the same fiber [27].

CONCLUSIONS

We demonstrated the first *in vivo* needle-based OCT of the prostate in these two patients to be safe and feasible. OCT images showed detailed images with an imaging depth of ~1.5 mm. The correlation of the OCT images with the biopsy is possible via 3D ultrasound registration and demonstrated different prostate tissue types such as regular atrophy, benign glands, adenocarcinoma Gleason 3, and stroma. This study opens the pathway towards *in vivo* needle-based OCT studies focusing on clinical relevance.

REFERENCES

1. Mottet N, Bellmunt J, Bolla M, et al. EAU-ESTRO-SIOG guidelines on prostate cancer. Part 1: screening, diagnosis, and local treatment with curative intent. Eur Urol 2017;71(4):618–629.
2. Smeenge M, De La Rosette JJMCH, Wijkstra H. Current status of transrectal ultrasound techniques in prostate cancer. Curr Opin Urol 2012;22(4):297–302.
3. Serefoglu EC, Altinova S, Ugras NS, Akincioglu E, Asil E, Balbay MD. How reliable is 12-core prostate biopsy procedure in the detection of prostate cancer? Can Urol Assoc J 2013;7(5–6):1–6.
4. Schoots IG, Petrides N, Giganti F, et al. Magnetic resonance imaging in active surveillance of prostate cancer: a systematic review. Eur Urol 2015;67(4):627–636.
5. Kasivisvanathan V, Rannikko AS, Borghi M, et al. MRI-targeted or standard biopsy for prostate-cancer diagnosis. N Engl J Med May 2018;378(19):1767–1777.
6. Schoots IG, Roobol MJ, Nieboer D, Bangma CH, Steyerberg EW, Hunink MGM. Magnetic resonance imaging-targeted biopsy may enhance the diagnostic accuracy of significant prostate cancer detection compared to standard transrectal ultrasound-guided biopsy: a systematic review and meta-analysis. Eur Urol 2015;68(3):438–450.
7. Wegelin O, van Melick HHE, Hooft L, et al. Comparing three different techniques for magnetic resonance imaging-targeted prostate biopsies: a systematic review of in-bore versus magnetic resonance imaging-transrectal ultrasound fusion versus cognitive registration. Is there a preferred technique? Eur Urol 2017;71(4):517–531.
8. Simmons LAM, Kanthabalan A, Arya M, et al. The PICTURE study: diagnostic accuracy of multiparametric MRI in men requiring a repeat prostate biopsy. Br J Cancer 2017;116(9):1159–1165.
9. Moldovan PC, Van den Broeck T, Sylvester R, et al. What is the negative predictive value of multiparametric magnetic resonance imaging in excluding prostate cancer at biopsy? A systematic review and meta-analysis from the European

Association of Urology Prostate Cancer Guidelines Panel. Eur Urol 2017;72(2):250–266.
10. Muller BG, de Bruin DM, van den Bos W, et al. Prostate cancer diagnosis: the feasibility of needle-based optical coherence tomography. J Med Imaging 2015;2(3):037501.
11. Freund JE, Buijs M, Savci-Heijink CD, et al. Optical coherence tomography in urologic oncology: A comprehensive review. SN Compr Clin Med 2018;1(2):67–84.
12. Muller BG, van Kollenburg RAA, Swaan A, et al. Needle-based optical coherence tomography for the detection of prostate cancer: a visual and quantitative analysis in 20 patients. J Biomed Opt 2018;23: 1–11.
13. Swaan A, Mannaerts CK, Scheltema MJV, et al. Confocal laser endomicroscopy and optical coherence tomography for the diagnosis of prostate cancer: A needle-based, in vivo feasibility study protocol (IDEAL phase 2A). J Med Internet Res 2018;20(5):1–2.
14. Krughoff K, Stone NN, Elliott J, Baer C, Arangua P, Crawford ED. 3D Biopsy: A New Method to Diagnose Prostate Cancer. In: Stone N, & Crawford E editors . The Prostate Cancer Dilemma. Cham: Springer, 2016 pp. 83–91.
15. Dangle PP, Shah KK, Kaffenberger B, Patel VR. The use of high resolution optical coherence tomography to evaluate robotic radical prostatectomy specimens. Int Braz J Urol 2009;35(3):344–353.
16. Swaan A, Muller B, Wilk L, et al. One-to-one registration of en-face optical coherence tomography attenuation coefficients with histology of a prostatectomy specimen. J Biophotonics 2018;12: e201800274.
17. Latchamsetty KC, Borden LS, Porter CR, et al. Experience improves staging accuracy of endorectal magnetic resonance imaging in prostate cancer: what is the learning curve? Can J Urol 2007;14(1):3429–3434.
18. Gaziev G, Wadhwa K, Barrett T, et al. Defining the learning curve for multiparametric magnetic resonance imaging (MRI) of the prostate using MRI-transrectal ultrasonography (TRUS) fusion-guided transperineal prostate biopsies as a validation tool. BJU Int 2016;117(1):80–86.
19. Rodriguez-Urrego PA, Cronin AM, Al-Ahmadie HA, et al. Interobserver and intraobserver reproducibility in digital and routine microscopic assessment of prostate needle biopsies. Hum Pathol 2011;42(1):68–74.
20. Jain M, Shukla N, Manzoor M, Nadolny S, Mukherjee S. Comment on "Modified full-field optical coherence tomography: A novel tool for rapid histology of fresh tissues". J Pathol Inform 2011;2(1):29.
21. Beuvon F, Dalimier E, Cornud F, Barry Delongchamps N. [Full field optical coherence tomography of prostate biopsies: A step towards pre-histological diagnosis?]. Prog Urol Jan. 2014;24(1):22–30.
22. Lopater J, Colin P, Beuvon F, et al. Real-time cancer diagnosis during prostate biopsy: ex vivo evaluation of full-field optical coherence tomography (FFOCT) imaging on biopsy cores. World J Urol 2016;34(2):237–243.
23. Faber DJ, van der Meer FJ, Aalders MCG, van Leeuwen TG. Quantitative measurement of attenuation coefficients of weakly scattering media using optical coherence tomography. Opt Express 2004;12(19):4353–4365.
24. Muller BG, Swaan A, de Bruin DM, et al. Customized tool for validation of optical coherence tomography in differentiation of prostate cancer. Technol Cancer Res Treat 2016;16: 1–9.
25. McCulloch P, Altman DG, Campbell WB, et al. No surgical innovation without evaluation: the IDEAL recommendations. Lancet 2009;374(9695):1105–1112.
26. De Fauw J, Ledsam JR, Romera-Paredes B, et al. Clinically applicable deep learning for diagnosis and referral in retinal disease. Nat Med 2018;24(9):1342–1350.
27. Beaudette K, Baac HW, Madore W-J, et al. Laser tissue coagulation and concurrent optical coherence tomography through a double-clad fiber coupler. Biomed Opt Express 2015;6(4):1293.